Journal of Alloys and Compounds 510 (2012) 125–133

Contents lists available at SciVerse ScienceDirect

Journal of Alloys and Compounds

journal homepage: www.elsevier.com/locate/jallcom

Effect of frozen spin on the magnetocaloric property of $La_{0.7}Ca_{0.3}CoO_3$ polycrystalline and single crystal samples

J.C. Debnath*, R. Zeng, J.H. Kim, P. Shamba, D.P. Chen, S.X. Dou

Institute for Superconducting and Electronic Materials, University of Wollongong, Northfields Ave., Wollongong, NSW 2522, Australia

ARTICLE INFO

Article history:
Received 14 March 2011
Received in revised form 30 August 2011
Accepted 30 August 2011
Available online 10 September 2011

Keywords:
Exchange-bias
Memory effect
Frozen spin
Magnetocaloric effect
Cluster-spin-glass

ABSTRACT

Polycrystalline (PC) and single crystalline (SC) samples of $La_{0.7}Ca_{0.3}CoO_3$ (LCCO) with the perovskite structure were synthesized by conventional solid-state reaction and the floating-zone growth method. We conducted isothermal magnetization measurements of the PC and SC samples at temperatures from 2.8 K to 140 K, and evaluated the magnetic entropy change ($-\Delta S_M$) under zero field cooling (ZFC) and field cooling (FC) to 2.8 K. An interesting result has been obtained, where the $-\Delta S_M$–T curves in the low temperature range show totally different features between the ZFC and FC cooling procedures. The $-\Delta S_M$ shows a large inverse irreversibility value for the ZFC process, while the $-\Delta S_M$ also shows a normal positive value, but one that is slightly larger at 2.8 K for the FC process for both samples. We also present the results of a comprehensive investigation of the magnetic properties of the LCCO system. Systematic measurements have been conducted on DC magnetization, AC susceptibility, and exchange-bias. These findings suggest that complex structural phases, including ferromagnetic and spin-glass/cluster-spin-glass (SG/CSG)) states and their transitions, exist in PC samples, while there is a much simpler magnetic phase regime in SC samples. It was also of interest to discover that the CSG induced a magnetic field memory effect and an exchange-bias-like effect.

© 2011 Elsevier B.V. All rights reserved.

1. Introduction

Rare-earth manganates of the general formula $Ln_{1-x}A_xMnO_3$ (Ln = rare earth, A = alkaline earth), possessing the perovskite structure, exhibit interesting properties such as colossal magnetoresistance, charge ordering, and electronic phase separation [1–5]. These properties of the manganates are strongly influenced by the average radius of the A-site cations, $\langle r_A \rangle$. Perovskite cobaltates of the type $Ln_{1-x}A_xCoO_3$ (Ln = rare earth, A = alkaline earth) are somewhat similar to the manganates [6–8]. Accordingly, many of the cobaltates show ferromagnetism and metallicity, depending on the composition and the size of the A-site cations. The cobaltates also show some unusual features in their magnetic properties.

Currently, there is an ongoing debate and increased research intensity on the magnetism of the $LaCoO_3$ system, due to the fascinating properties of compounds in this family and possible multifunctional applications [9–16]. The main controversial points are concerned with the spin states (low to intermediate/high spin), magnetic behaviors (phase separation and spin glass (SG) state), and transitions between them. It is commonly accepted that the ground state of $LaCoO_3$ is a non-magnetic insulator. It is commonly considered that with increasing temperature, a paramagnetic insulating state continuously develops above 50 K, and an insulator-to-metal transition is observed around 500 K [15]. There has been controversy over the nature of the high-temperature spin state, namely, whether it is high-spin (HS), intermediate-spin (IS), or even a mixture of both [16].

The $La_{1-x}Ca_xCoO_3$ system has been studied by many groups [16–25]. The substitution of Ca^{2+} on La^{3+} sites oxidizes part of the Co^{3+} into Co^{4+}. The spin configuration of Co^{4+} has been proposed by different investigators to be low spin (LS) ($t_{2g}^5\ e_g^0$, $S = 1/2$), HS ($t_{2g}^3\ e_g^2$, $S = 5/2$), and even IS ($t_{2g}^4\ e_g^1$, $S = 3/2$), depending on the Ca content and temperature [14,16]. The theoretical effective magnetic moment (μ_{eff}) of Co^{3+} and Co^{4+} in the LS, IS, and HS states are 0, 2.83, and 4.90 μ_B, and 1.73, 3.87, and 5.92 μ_B, respectively [19–25].

Many efforts have been made to determine the influence of Co addition on the magnetic and electrical transport properties and magnetocaloric effect (MCE) in various materials. Roy and Das [26] investigated the effects of particle size on the electrical transport and magnetic properties of $La_{0.5}A_{0.5}CoO_3$ (A = Sr, Ca, and Ba) nanoparticles. The magnetization results indicate that Co^{3+} ions are in the intermediate spin state, but Co^{4+} ions exist in a mixture of intermediate and high spin states. The observed frequency dependent shoulder in the in-phase and the peak in the out-of-phase component of the AC susceptibility indicate the glassy nature

* Corresponding author. Fax: +61 2 4221 5731.
E-mail address: jcd341@uowmail.edu.au (J.C. Debnath).

0925-8388/$ – see front matter © 2011 Elsevier B.V. All rights reserved.
doi:10.1016/j.jallcom.2011.08.104

of the samples. The analysis of the AC magnetization results suggests that the magnetic behavior is consistent with the cluster glass model. Debnath et al. [27] measured the effect of Co substitution on the MCE in $La_{0.7}Ca_{0.3}MnO_3$ and found that the entropy change value decreases slightly (3.163 for $La_{0.7}Ca_{0.3}Mn_{0.95}Co_{0.05}O_3$ and 4.63 J/(kg K) for $La_{0.7}Ca_{0.3}MnO_3$ at 1 T), but the relative cooling power is enhanced by about 41% due to small changes from Co doping. The effects of Co substitution on the magnetocaloric effect in $La_{0.67}Pb_{0.33}Mn_{1-x}Co_xO_3$ were measured by Dhahri et al. [28]. It was found that the maximum change in magnetic entropy for $La_{0.67}Pb_{0.33}Mn_{0.7}Co_{0.3}O_3$ is 3.22 J/(kg K) at Curie temperature, T_C = 260 K for a magnetic field change of 1 T. The magnetic field and temperature dependence of the magnetic susceptibility of $La_{0.9}Ca_{0.1}CoO_3$ single crystal has been measured by Szymczak et al. [29]. The irreversibility line characteristic of spin-glass-like systems was identified on the *H*–*T* plane. It was shown that the magnetic moments in this lightly doped crystal freeze into a cluster spin glass state. Magnetic properties of the $La_{0.9}Ca_{0.1}CoO_3$ single crystals have been described in terms of a spin-state transition of the Co^{3+} ions with increasing temperature from a LS ground state to an IS excited state, with energy gap Δ = 268 K.

Direct and inverse magnetocaloric effects in A-site ordered $PrBaMn_2O_6$ manganite have been observed by Aliev et al. [30]. These direct and inverse MCE are observed at the corresponding Curie and Néel points. The value of the inverse MCE in the heating run is less than in the cooling regime. This effect can be attributed to competition between ferromagnetic and antiferromagnetic interactions. Inverse and direct magnetocaloric properties were also observed by Ma et al. [31] in melt-spun and annealed $Ni_{42.7}Mn_{40.8}Co_{5.2}Sn_{11.3}$ ribbons. The maximum inverse and direct magnetic entropy change values (ΔS_M) were −1.3 and 6.8 J/(kg K) for a melt-spun and −1.6 and 32.8 J/(kg K) for an annealed sample for a field change of 1 T. The magnetic properties and magnetocaloric effect (MCE) in $GdCo_3B_2$ have been studied by Li et al. [32]. The compound undergoes a magnetic Co–Co ordering at ∼160 K, and a second magnetic Gd–Gd ordering transition at 54 K. A reversible magnetocaloric effect has been observed, accompanied by a second-order phase transition at around the Gd–Gd sublattice ordering temperature. The values of maximum magnetic entropy change ($-\Delta S_M$) reach 5.0 and 11.6 J/(kg K) for field change of 2 and 7 T, respectively, with no obvious hysteresis loss around 56 K. A field-induced MCE conversion is observed in $CoCl_2$, associated with the field-induced transition from the antiferromagnetic (AFM) to the ferromagnetic (FM) state by Liu et al. [33]. The value of the magnetic-entropy change, 4.1 and 11.5 J/(kg K) at 27 K for a field change of 3 and 7 T, respectively, but below the Néel temperature, T_N, for small magnetic field change 2.1 T, shows inverse MCE.

The structural and magnetic properties of $MnCo_{1-x}V_xGe$ (x = 0.00, 0.02, 0.04, 0.06, 0.08, 0.10, 0.20, and 0.30) compounds were investigated by Meng et al. [34]. The magnetization measurements show that the $MnCo_{1-x}V_xGe$ compounds exhibit complex magnetic behavior. The Curie temperature can be tuned from 360 K to 148 K by increasing x. The maximal magnetic-entropy change is 3.9 J/(kg K) for x = 0.06 at a field change from 0 to 1.5 T at about 265 K. The spin-reorientation and magnetocaloric properties in $Nd_{1-x}Dy_xCo_4Al$ (x = 0, 0.1) alloys were investigated by Ma et al. [35]. These alloys undergo two successive spin-reorientation transitions around room-temperature, which results in a positive and negative magnetic entropy change, respectively. The maximum values of entropy change for $Nd_{0.9}Dy_{0.1}Co_4Al$ are 0.15 and −0.88 J/(kg K) for a field change of 7 kOe and 30 kOe at the temperatures of 305 and 317 K, respectively. The influence of Co addition on the magnetic properties and magnetocaloric effect of $(Fe_{1-x}Co_x)_{75}Nb_{10}B_{15}$ (x = 0.15 and 0.30) powders has been studied by Ipus et al. [36]. The temperature dependence of magnetization curves shows that the Curie temperature of the amorphous phase increases as the Co content increases. The peak magnetic entropy change slowly increases with Co addition for low crystalline fractions, and the refrigerant capacity decreases as Co increases.

Since the magnetic and electrical properties of rare earth transition metal oxides with perovskite structure are strongly dependent on the valence state and spin state of the metal ions, and on the defects, these make the materials' magnetic properties very sensitive to sample preparation conditions and processing. It will be worthwhile to compare the properties of a single crystalline (SC) sample with those of a bulk polycrystalline (PC) sample prepared by the conventional solid-state reaction method. In the present work, we have prepared PC and SC $La_{0.7}Ca_{0.3}CoO_3$ (LCCO) samples with the same composition of starting raw powders, determined the magnetic properties, and analyzed the differences between these two types of samples. Interestingly, an anomalous magnetic field memory effect, an exchange-bias-like effect, and a large inverse irreversible magnetocaloric effect have been observed in this system. We propose that compositional inhomogeneity is the predominant source of the magnetic properties and magnetocaloric effect.

2. Experimental

PC and SC $La_{0.7}Ca_{0.3}CoO_3$ (LCCO) samples with the perovskite structure were synthesized by conventional solid-state reaction and the floating-zone growth method. Powder samples of $La_{0.7}Ca_{0.3}CoO_3$ were synthesized using the standard solid-state reaction method at high temperature, by mixing La_2O_3, $CaCO_3$, and Co_3O_4 with up to 99.9% purity in the desired proportions. The starting materials were intimately mixed in an agate mortar and first fired at 700 °C for 12 h. Then, the mixture was reground and again fired at 900 °C for 12 h. Finally, the sample was again reground, pressed into pellets, and sintered at 1100 °C for 24 h.

For the SC sample, as-grown single phase powders were then hydrostatically pressed into feed and seed rods with a diameter of 6 mm and a length of about 90 mm. The rods were sintered at 1200 °C for 6 h. The crystal growth was performed in an infrared furnace equipped with four 1000 W halogen lamps, and the single crystal was grown in 30 cc/min oxygen flow rate. To avoid Co evaporation during the growth, we use oxygen flow in the synthesis process for a SC sample. Crystal wafers were cut perpendicular to the growth direction and polished to a mirror finish to allow us to examine them for the presence of macroscopic defects such as cracks, twins, or grain boundaries and inclusions under a polarized microscope. Cu Kα X-ray diffraction (XRD) of wavelength λ = 1.540562 Å was used for XRD measurements to check the phase purity and the crystal structure. Single crystal XRD was carried out on the polished surface of the rectangular crystal samples to examine the crystal quality and orientation of the crystal growth. The measurements were conducted in a θ–2θ scan mode in the 2θ range of 10–60° for single crystal measurements. Cu Kα radiation was used as the X-ray source. Typical XRD patterns obtained from the single crystal are shown in Fig. 1(b). All the peaks of each pattern can be indexed by the (h 0 0) diffraction peaks of $La_{0.7}Ca_{0.3}CoO_3$. No traces of impurities or inclusions were obtained in our crystal sample. The composition has been checked using energy dispersive X-ray analysis (EDX) and Raman spectroscopy and the results confirm the composition within experimental errors. A rectangular piece of the crystal was cut, and the magnetization measurements were performed using a physical properties measurement system (PPMS, 14 T) in the temperature range of 5–300 K. To restore the sample to the same demagnetized initial state, the sample was warmed up to 300 K after the measurement of each hysteresis loop. The entropy change was evaluated from the magnetization isotherms.

3. Results and discussion

The phase composition and crystal structure of the samples were characterized by X-ray diffraction (XRD), and the results confirmed their high purity and perovskite structure. The XRD patterns of the PC and SC $La_{0.7}Ca_{0.3}CoO_3$ (LCCO) samples are shown in Fig. 1. The XRD results on these LCCO samples (Fig. 1) indicate that the PC sample is in the orthorhombic (space group: *Pnma*) phase (O phase), while for the SC sample, a single-phase diffraction pattern was obtained, yielding a rhombohedral structure with the *R*-3*C* space group [37]. The appropriate structure for x > 0.2 may be orthorhombic as given in Ref. [14]. However, our X-ray analysis could not distinguish the rhombohedral distortion that is assumed here from a slightly more distorted orthorhombic structure.

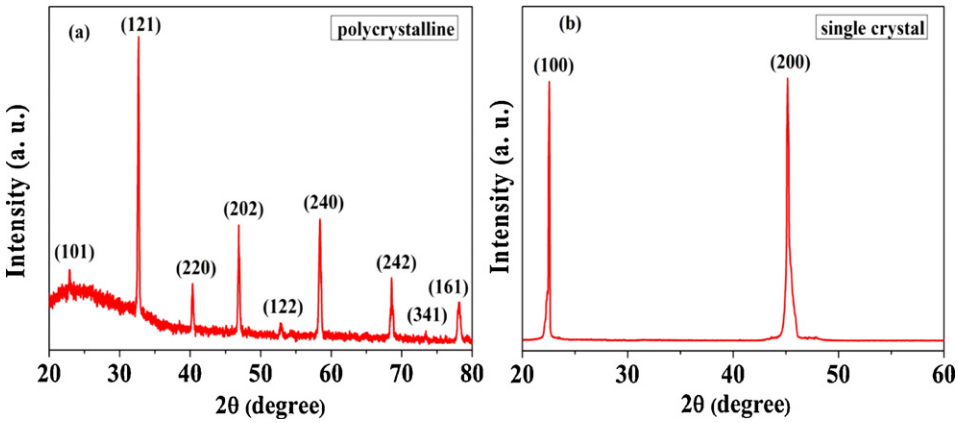

Fig. 1. XRD patterns for both polycrystalline (a) and single crystal (b) samples of $La_{0.7}Ca_{0.3}CoO_3$.

The EDX and Raman spectra are shown in Fig. 2. The EDS spectrum (Fig. 2(a)) shows that the products are composed of La, Ca, Co, and O, and it confirms the composition within experimental errors. The C peak in the spectrum is attributed to the carbon tape of the sample holder. The Raman scattering of pure $La_{0.7}Ca_{0.3}CoO_3$ is shown in Fig. 2(b). Four bands belonging to the cobaltite structure are observed at 156, 462, 551, and 672 cm^{-1} (~156 cm^{-1} – rare earth internal vibration mode; ~462 cm^{-1} – O–O octahedral rotation; ~551 cm^{-1} – Co–O bending vibration; ~ cm^{-1} – Co–O stretching vibration), and the peaks at ~299, ~406, and 626 cm^{-1} are for CaCoO [38–40].

The temperature dependence of the zero-field-cooled (ZFC) and field-cooled (FC) magnetization was measured for both the PC powder and the single crystal (SC) samples. For all the results on the present SC sample, the applied fields were parallel to the *c*-axis. The results are replotted as DC susceptibility and inverse susceptibility in Fig. 3(a and b). A sharp increase in the magnetization occurs in the low-field FC data around the Curie temperature, $T_C \approx 102$ K for the poly-crystalline and 104 K for the single-crystal sample, indicating that the system has become ordered and attained a spontaneous magnetization. A characteristic strong irreversibility between the low-field ZFC and FC magnetization curves appears just below the transition temperature. It is suggested that this irreversibility possibly arises due to the canted nature of the spins or due to the random freezing of spins. The peculiar shape of the χ–T curves suggests a complex magnetic structure below T_C. The ZFC curve of the PC sample shows two small peaks, one at 80 K and a second anomaly around 35 K as a relatively sharp maximum, accompanied by a change in the slope of the FC magnetization curve, indicating a transition in the ordered spin structure. The single-crystal sample shows much simpler transitions compared to the PC ones, while the ZFC curve shows only one similar peak around 90 K (Fig. 3(b)). At high temperatures (higher than T_C), there may be a first order structural phase transition at temperature, $T_{ST} \approx 250$ K (Fig. 3(a)) for the PC sample, and $T_{ST} \approx 160$ K (Fig. 3(b)) for the single-crystal sample, which are induced by spin state changes (from lower spin state to higher spin state), since the slope of the $1/\chi - T$ curves is changed and the effective magnetic moment (μ_{eff}) increases after the transition (Fig. 3(a) and (b)). Above the transition temperature, both samples show Curie–Weiss behavior, and a fit to the Curie–Weiss law yields a ferromagnetic (FM) μ_{eff}, the values of which are listed in Fig. 3(a) and (b). The values of μ_{eff} below and above T_{ST} are 3.01 μ_B and 3.32 μ_B for the PC, and 2.66 μ_B and 3.06 μ_B for the SC sample. For both samples, the effective magnetic moment (μ_{eff}) above the structural phase transition temperature (T_{ST}) is higher than the magnetic moment which is measured below the T_{ST}, indicating that the spin state changes are from a lower spin state to a higher spin state.

Fig. 4 shows the difference in the magnetization between the ZFC and FC processes for both the polycrystalline and the single crystal samples. In the low temperature range, the magnetization difference is obvious, which may be due to the effects of the exchange bias behavior of the material.

We have conducted AC susceptibility measurements on the PC sample in the temperature range of 5–150 K. The in-phase and out-of-phase susceptibility versus temperature curves are shown in Fig. 5(a) and (b). The AC susceptibility shows more complex spin states and phase transitions, and we can detect 6 significant transition temperatures, as is shown in Fig. 5(b): $T_1 = 124$ K, $T_2 = 102$ K, $T_3 = 93$ K, $T_4 \approx 53.6$–58 K, $T_5 \approx 31$–34 K, and $T_6 = 20.5$ K. We suggest that T_1 may be another structural phase transition temperature (for lower Ca^{2+} concentration). T_2 is the Curie temperature, T_C. The T_4 temperature range represents the temperature for the appearance of SG, since it is strongly dependent on the AC frequency. T_3 and T_5 relate to the two peaks in Fig. 3(a): these are the temperatures at which antiferromagnetic (AFM) interactions appear due to the high spin (HS) or intermediate spin (IS) to low spin (LS) transitions. T_6 is the low spin transition temperature. It should be noted that T_5 has an AC frequency dependence since it coexists with spin glass in this temperature range.

Although ferromagnetic (FM) interactions dominate the magnetic transitions, AFM interactions also exist between Co ions. This is because the system phase may separate into hole-rich FM clusters dominated by the FM double exchange interaction between Co^{3+} and Co^{4+}, with the clusters embedded in a hole-poor non-FM matrix. This matrix is dominated by the Co^{3+}–Co^{3+} interaction, which is known to be AFM superexchange, (However, Co–Co magnetic interaction depends on the spin state, e.g. Co^{3+} IS–IS is FM and Co^{3+} HS–HS is AFM), as with the Co^{4+}–Co^{4+} interaction. The coexistence of and competition between FM and AFM interactions could lead to SG-like behavior. Crystallographic inhomogeneity, stoichiometric inhomogeneities, and the Co ion spin-state transitions heighten the co-existence of the FM and AFM interactions, and bring about magnetic phase separation in the samples, which is similar to the situation in the Sr-doped system [25]. It is highly probable that the crystallographic homogeneity and the stoichiometric homogeneity in the PC sample are much lower than in the SC sample, which leads to much more complex magnetic behavior in the PC sample.

M–*H* loops were collected at different temperatures under ZFC and FC with different sweep fields. A large hysteresis loop develops below T_C and attains a larger remanence value (M_R) and higher coercive force (H_C) at the lowest temperature. The material becomes harder with decreasing temperature, with the coercive field increasing monotonically with decreasing temperature. The difference between the PC and the SC samples is that the loops or

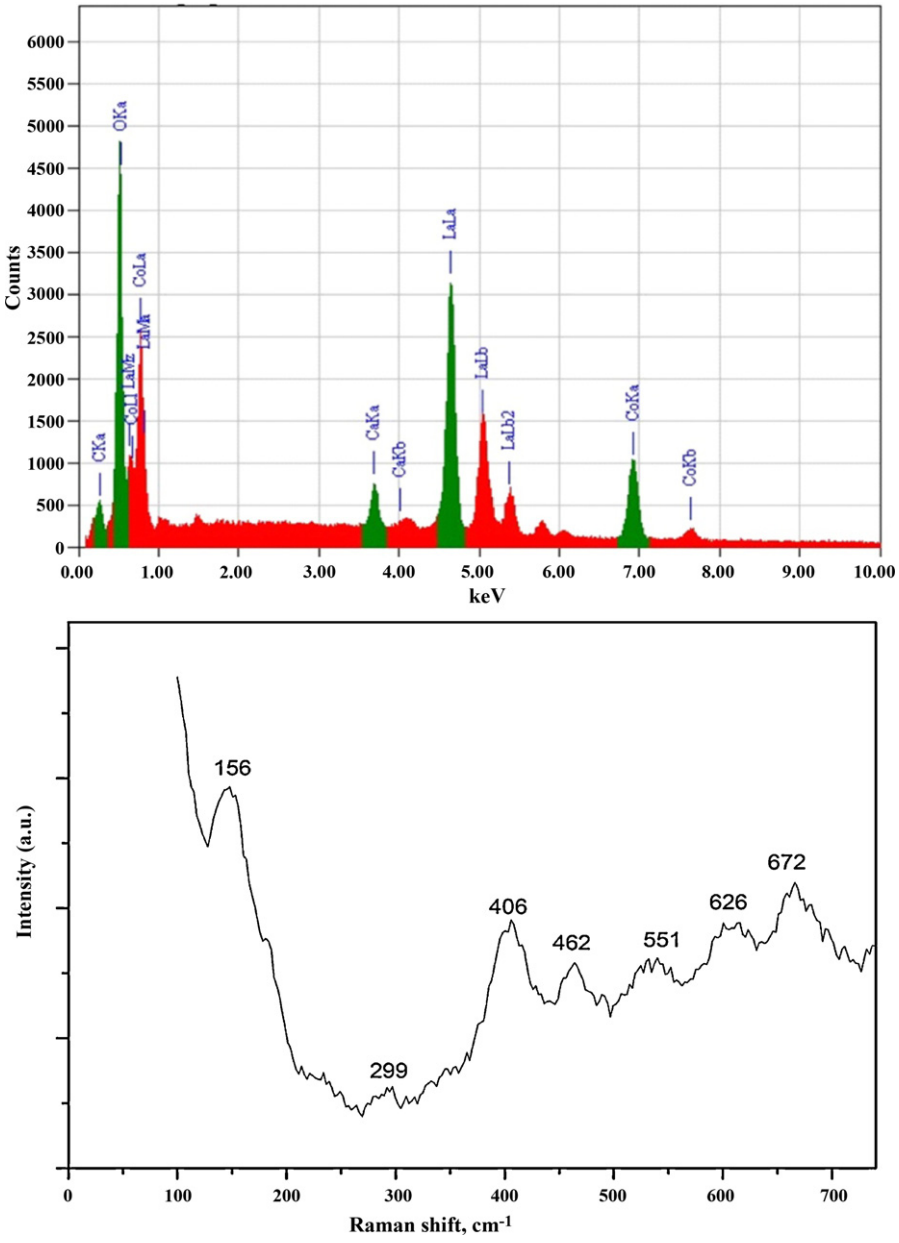

Fig. 2. EDX spectrum (a) and Raman spectra of $La_{0.7}Ca_{0.3}CoO_3$.

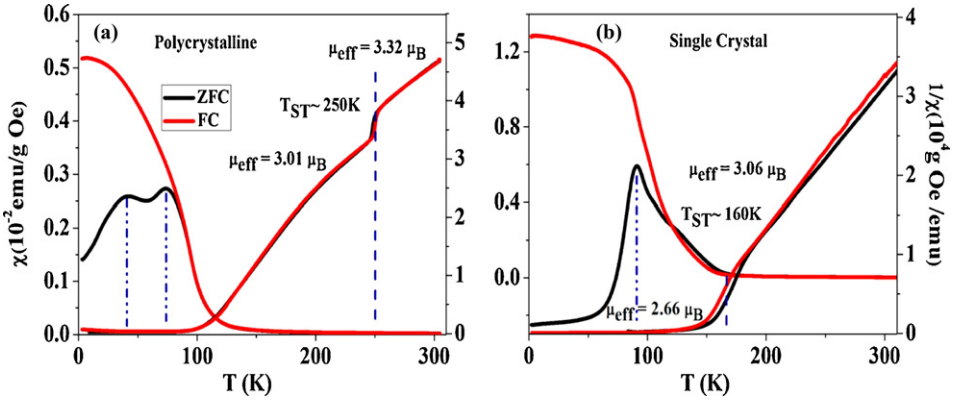

Fig. 3. DC and inverse susceptibility (χ and $1/\chi$) versus T curves under zero-field cooling (ZFC) and after field cooling (FC) at a field of 1 kOe. For the PC sample (a) and for the SC sample (b).

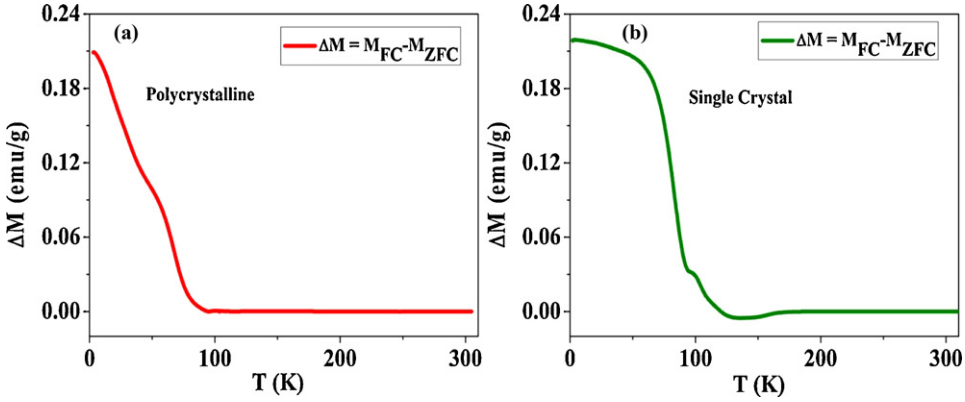

Fig. 4. Magnetization difference between ZFC and FC processes: polycrystalline (a) and single crystal (b).

curves of the SC sample appear straighter and show sharp changes in all the *M*–*H* loops, while all the values of M_R and H_C for the SC are larger than the corresponding PC ones.

For clarification, we have selected the 10 kOe and 20 kOe sweep field loops as examples, which are shown in Fig. 6. It is interesting to note that, in the left panels, Fig. 6(a) and (c), for sweep field of 1 T, less than the field cooling field of 1.5 T, the ZFC *M*–*H* loops are closed, while the FC *M*–*H* loops are not closed and are also upshifted. The non-closed loop phenomenon is typical SG relaxation behavior, while the upshifts are mainly due to the FM M_R behavior. We suggest that the SG, or more likely here, the cluster spin glass (CSG), has also significantly contributed to the up- or downshifts. In the right panels, Fig. 6(b) and (d), for a sweep field of 2 T, greater than the field cooling field of 1.5 T, both the FC and ZFC *M*–*H* loops are closed, but the *M*–*H* loops are still up-/downshifted, with the values lower than for the left panel ones. The up-/downshifts of the *M*–*H* loops are attributed to exchange bias – like behavior (M_{EB}), and the values of M_{EB} are listed in Fig. 6. Moreover, the left-/right-shifts of the *M*–*H* loops are attributed to exchange bias (H_{EB}), and the values of H_{EB} are listed in Fig. 6(b) and (d). For the origin of the exchange bias, we note that Luo and Wang [41] have observed similar shifts on both axes, representing exchange bias – like phenomena, although there have been later arguments about this [42], however, our results suggest that, except for the minor hysteresis loops, the freezing properties of local anisotropy in a CSG system make a significant contribution to both shifts. Moreover, the grain boundaries in PC samples can enhance the exchange bias, so that the H_{EB} in the PC sample (in Fig. 6(b)) > H_{EB} in the single-crystal sample (in Fig. 6(d)), even though the H_C of the PC sample is less than the H_C of the SC sample.

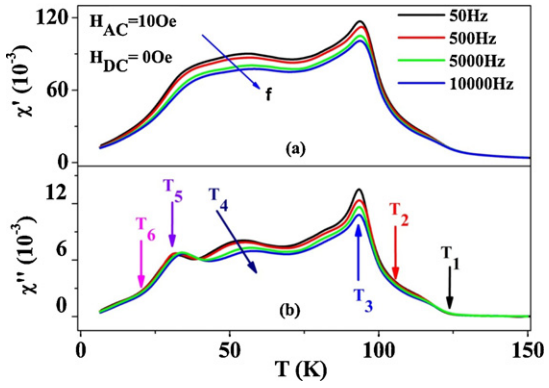

Fig. 5. In-phase χ' and out-of-phase χ'' AC susceptibility versus *T* curves at different frequencies over a temperature range of 5–150 K for the PC sample: (a) χ'–*T* curves and (b) χ''–*T* curves.

The magnetization (*M*–*H*) curves of the PC and SC samples, measured with different sweep fields after ZFC and 1.5 T FC to 10 K, are shown in Fig. 7. Different magnetic field-memory effects were observed after ZFC and 1.5 T field cooling. It should be noted that all the *M*–*H* curves exhibit a kink or step, where the field position is the same as the maximum field value of the last sweep field. For the ZFC *M*–*H* curves in the left panels of Fig. 7(a) and (c), the kinks or the steps are increased step by step with increasing sweep field. For the *M*–*H* curves after 1.5 T FC in the right panels of Fig. 7(b) and (d), the kinks are increased step by step with increasing sweep field, although the steps go down when the sweep field is less than the 1.5 T FC field, but increase back up to the first field sweep M_R level when the sweep field is greater than the 1.5 T FC field. These demonstrate the feature that the kink value (field value) always coincides with (remembers) the last forward maximum sweep field value – we define it as the magnetic field memory effect. This effect is possibly due to a combination of hard FM typical clusters showing SG behavior and frozen spin behavior.

In order to obtain more information on properties of the magnetic clusters, we have measured the magnetization in the polycrystalline (PC) and single crystalline (SC) samples as a function of magnetic field in the ZFC regime over a wide range of temperatures. Fig. 8 shows, as an example, the *M*–*H* dependences measured at 50–110 K for the PC and SC samples. According to the procedure proposed by Yamaguchi et al. [21] and Sun et al. [43], the results were fitted to the following functional dependence obtained in the molecular field approximation:

$$M(H) = NgS\beta B_s\left(\frac{g\beta S(H+\lambda M)}{kT}\right) + \lambda_0 H \quad (1)$$

where *N* is the number of clusters with effective spin *S* per formula unit, B_s is the Brillouin function, β is the Bohr magneton, and λ is a molecular field constant. Unfortunately, no good fittings were obtained while assuming that the effective spin *S* does not depend on the magnetic field value *H*. To describe the experimental data, one needs to assume that *S* increases with increasing *H*. It confirms the concept of electronic-phase separation based on the presence of small clusters with mobile phase boundaries [44].

In order to evaluate the magnetocaloric effect (MCE), the isothermal magnetization curves of the PC and SC samples were measured with a field step of 0.05 mT in the magnetic field range of 0–1.5 T and over the large temperature range of 20–140 K. Such families of *M*–*H* curves are shown in Fig. 9. The curves reveal low variation in the magnetization around the Curie temperature for both samples, indicating that there is little possibility of obtaining a large magnetic entropy change associated with the ferromagnetic to paramagnetic transition occurring at T_C.

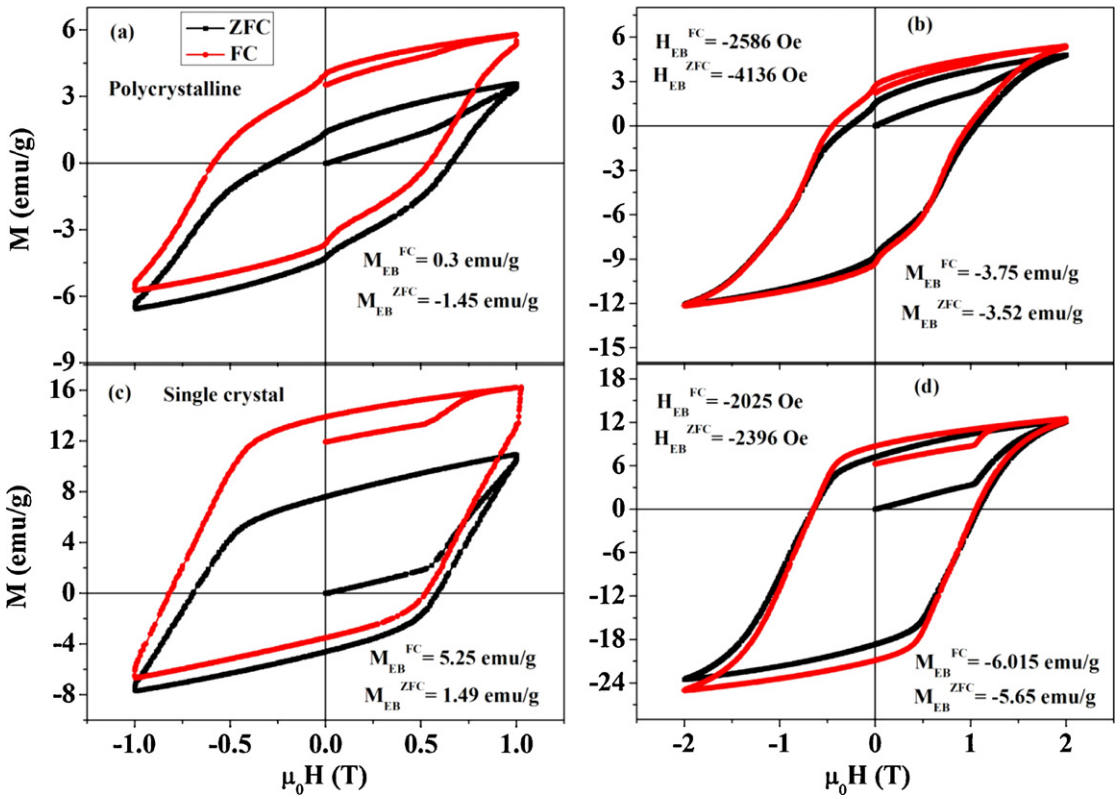

Fig. 6. *M–H* loops of $La_{0.7}Ca_{0.3}CoO_3$ PC ((a) and (b)) and single-crystal ((c) and (d)) samples after ZFC and 1.5 T FC to 5 K. Different sweep fields were used, lower or higher than the cooling field of 1.5 T, and they revealed different loop shifting features, representing exchange-bias-like phenomena.

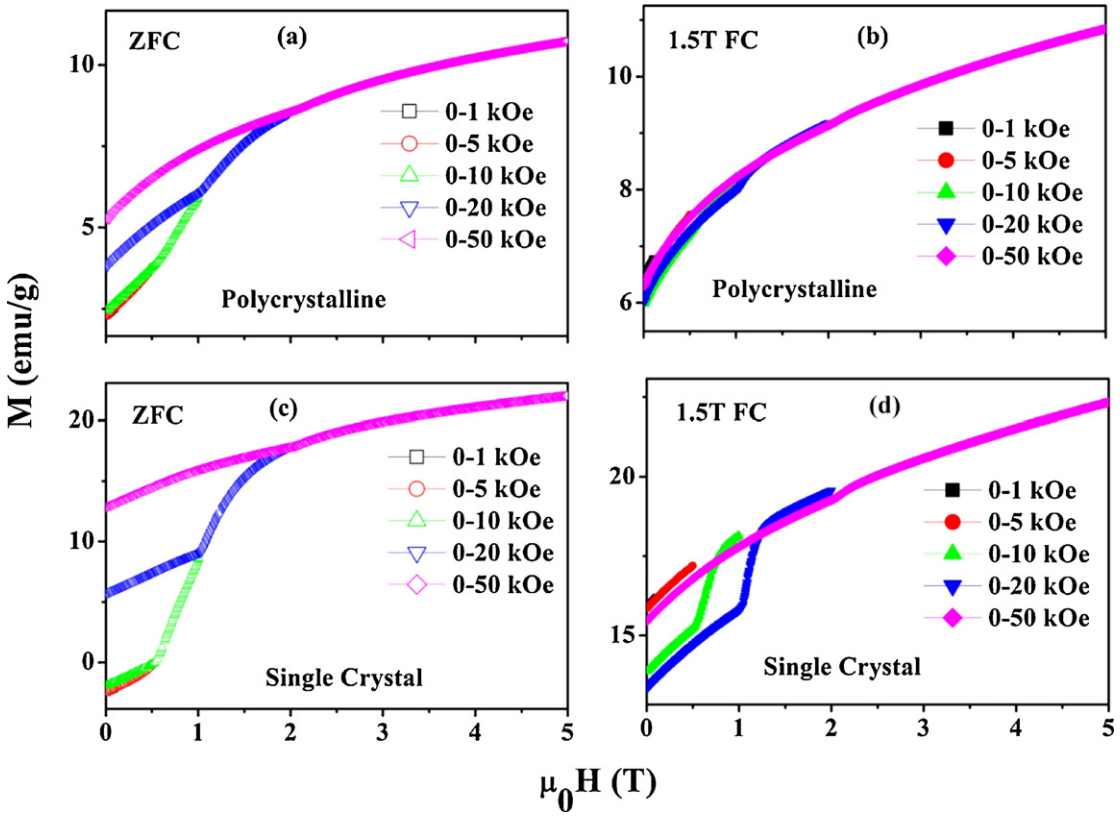

Fig. 7. *M–H* curves of $La_{0.7}Ca_{0.3}CoO_3$ polycrystalline ((a) ZFC and (b) FC) and single-crystal ((c) ZFC and (d) FC) samples with different sweep fields after ZFC and 1.5 T FC to 10 K. Different magnetic field-memory effects were observed after ZFC and 1.5 T field cooling.

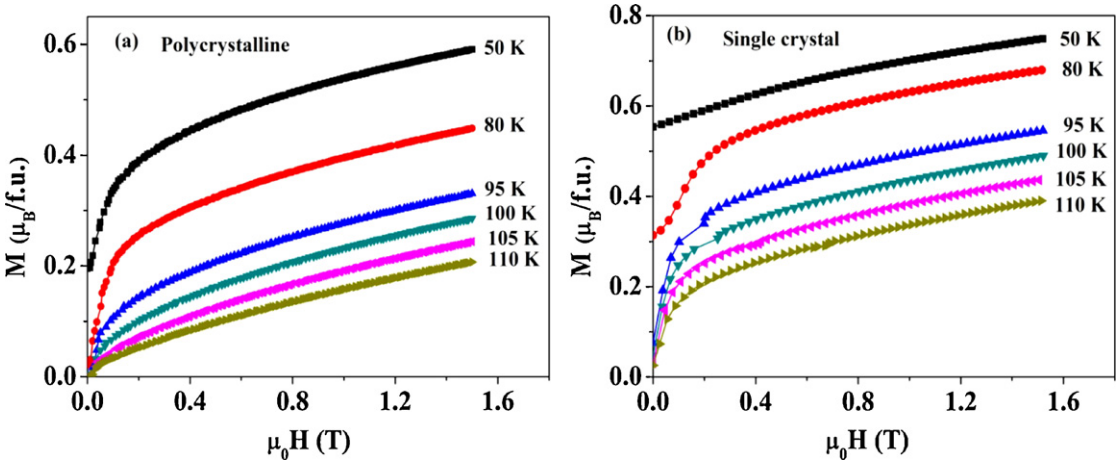

Fig. 8. Magnetization curves at 50, 80, 95, 100, 105, and 110 K for PC and SC $La_{0.7}Ca_{0.3}CoO_3$ samples.

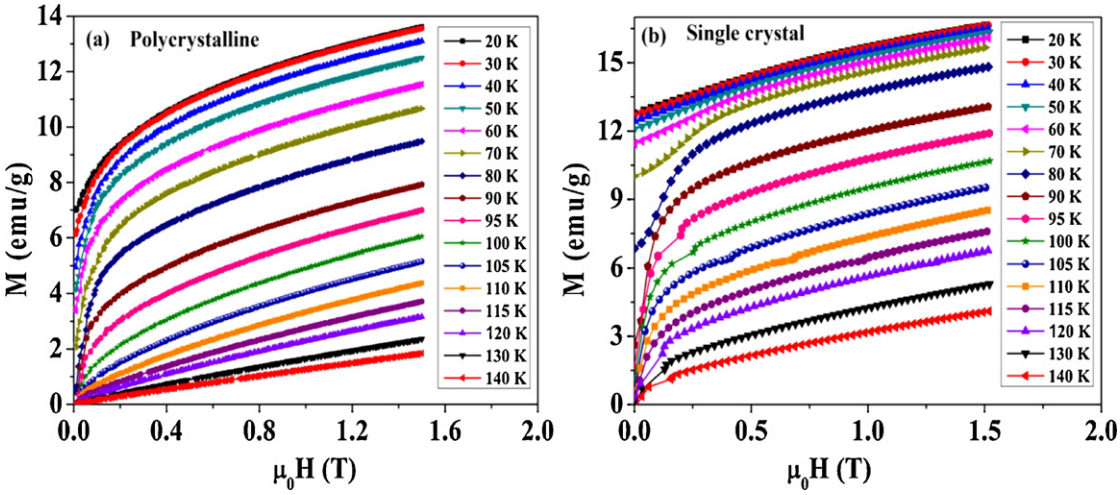

Fig. 9. Magnetization evolution versus applied magnetic field at several temperatures for PC and SC $La_{0.7}Ca_{0.3}CoO_3$ samples.

To understand the nature of the magnetic transition in the samples, Arrott plots of M^2 versus H/M (not shown), covering a broad temperature range around T_C, have indicated that the transition is second order.

The magnetic entropy change ($-\Delta S_M$) versus temperature under ZFC and FC to 2.8 K at 1.5 T field was derived for both samples from the calculated isothermal magnetic entropy change $-\Delta S_M$ from isothermal magnetization curves, according to the Maxwell equation. We found that the frozen spins have a significant influence on the $-\Delta S_M$. An interesting result is presented in Fig. 10, where the $-\Delta S_M$–T curves in the low temperature range show totally different features between the ZFC and FC cooling pro-

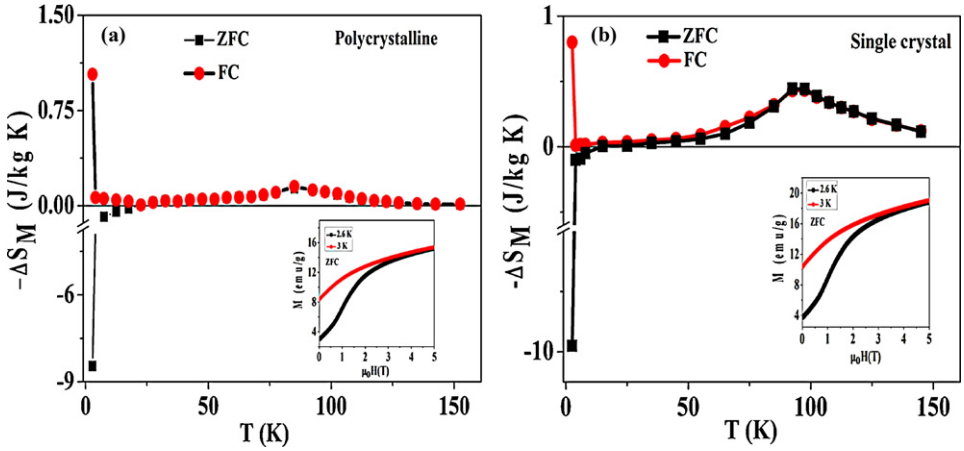

Fig. 10. Magnetic entropy changes ($-\Delta S_M$) versus temperature curves for 0–1.5 T field change for PC (a) and SC (b) samples. Insets: M–H loops of $La_{0.7}Ca_{0.3}CoO_3$ PC and SC samples for 2.6 K and 3.0 K, respectively.

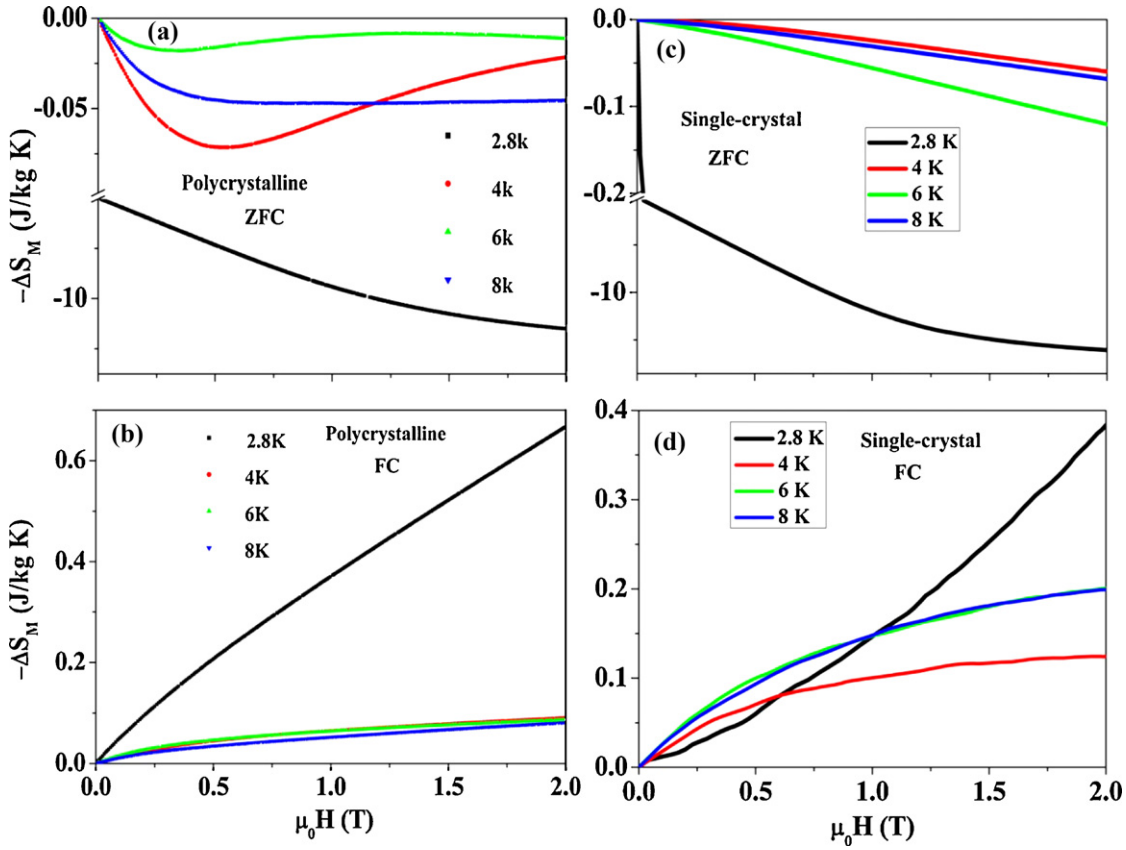

Fig. 11. $-\Delta S_M$–H curves at 2.8 K, 4 K, 6 K, and 8 K under field change of 0–2 T after ZFC and 2 T field cooling to 2.8 K for the PC sample ((a) and (b)) and for the SC sample ((c) and (d)).

cedures. The $-\Delta S_M$ shows a large inverse irreversibility value for the ZFC process, since there are a large amount of unfrozen spins aligned under the external field in the low temperature range, while the $-\Delta S_M$ shows a normal positive value, and there is a slightly larger $-\Delta S_M$ value at 2.8 K, which indicates that a small amount of unfrozen spins still exist. The interesting thing is that at 2.8 K, both the PC and the SC samples show a large inverse irreversibility value for the ZFC process, which is about 8.1 J/(kg K) and 9.8 J/(kg K), respectively, whereas for the FC process, this value is very small, about 1 J/(kg K) for both samples. Another feature is that at or near T_C, this entropy change value is negligible, even compared to the low temperature value. We suggest that the higher entropy change value at lower temperature is due to the significant influence of the frozen spins on the $-\Delta S_M$.

To determine the behavior of the samples at lower temperatures, we have measured the entropy change values at 2.8 K, 4 K, 6 K, and 8 K under a field change of 0–2 T after ZFC to 2.8 K, which are shown in Fig. 11. These $-\Delta S_M$–H curves after ZFC to 2.8 K show more complex behavior than the FC ones. In the ZFC process, the PC bulk sample shows pronounced curvature in its $-\Delta S_M$–H curves at the temperatures of 4 K, 6 K, and 8 K, whereas for the single crystal, no curvature behavior is observed at these temperatures. So, we think that further detailed investigation is necessary to explain these peculiar properties.

As suggested by our results, the cluster spin glass (CSG) system confirms the presence and contribution of the freezing properties of the local anisotropy of the material on the MCE. So we can draw the conclusion that this interesting MCE property of this material is influenced by the effect of frozen spins.

4. Conclusions

We have measured the magnetic entropy change ($-\Delta S_M$) under ZFC and FC processes. An interesting result is obtained at low temperature, where the $-\Delta S_M$ shows a very large inverse irreversibility value for the ZFC process, while the $-\Delta S_M$ shows a normal positive value and a slightly larger $-\Delta S_M$ value at 2.8 K for the FC process. We also have demonstrated several types of complex and fascinating magnetic behavior in the LCCO system, which will possibly be useful for multifunctional applications. The magnetic properties in this system strongly depend on the sample preparation processing and conditions. From comparing the magnetic behaviors in PC and SC samples, we propose that compositional inhomogeneity (mainly Ca^{2+} content) leads to complex variations in the Co ion valence and spin states, which then lead to the strong spin-glass/cluster-spin-glass behavior which significantly influences the magnetic properties of this system.

Acknowledgement

This work is supported by the Australian Research Council through a Discovery project (project ID: DP0879070).

References

[1] C.N.R. Rao, B. Raveau (Eds.), Colossal Magnetoresistance, Charge Ordering and Related Properties of Manganese Oxides, World Scientific, Singapore, 1998.
[2] Y. Tokura (Ed.), Colossal Magnetoresistance Oxides, Gorden and Breach, London, 1999.
[3] A.P. Ramirez, J. Phys: Condens. Matter 9 (1997) 8171.
[4] E. Dagotto (Ed.), Nanoscale Phase Separation and Colossal Magnetoresistance, Berlin, Springer, 2003.

[5] C.N.R. Rao, P.V. Vanitha, Curr. Opin. Solid State Mater. Sci. 6 (2002) 97.
[6] G.H. Jonker, J.H. Van Santen, Physica 19 (1953) 120.
[7] C.N.R. Rao, O. Parkash, D. Bahadur, P. Ganguly, S. Nagabhushana, J. Solid State Chem. 22 (1977) 353.
[8] M.A. Senaris-Rodriguez, J.B. Goodenough, J. Solid State Chem. 118 (1995) 323.
[9] P.M. Raccah, J.B. Goodenough, Phys. Rev. 155 (1967) 932.
[10] J.M. Tranquada, B.J. Sternlleb, J.D. Axe, Y. Nakamura, S. Uchida, Nature 375 (1995) 561.
[11] M. Fäth, S. Freisem, A.A. Menovsky, Y. Tomioka, J. Aarts, J.A. Mydosh, Science 285 (1999) 1540.
[12] C. Renner, G. Aeppli, B.-G. Kim, Y. Soh, S.-W. Cheong, Nature 416 (2002) 518.
[13] A.L. Chernyshev, A.H. Castro Neto, A.R. Bishop, Phys. Rev. Lett. 84 (2000) 4922.
[14] J.C. Burley, J.F. Mitchell, S. Short, Phys. Rev. B 69 (2004) 054401.
[15] E. Dagotto, J. Burgy, A. Moreo, Solid State Commun. 126 (2003) 9.
[16] (a) M. Imada, A. Fujimori, Y. Tokura, Rev. Mod. Phys. 70 (1998) 1039; (b) D. Phelan, D. Louca, K. Kamazawa, M.F. Hundley, K. Yamada, Phys. Rev. B 76 (2007) 104111.
[17] M. Kriener, C. Zobel, A. Reichl, J. Baier, M. Cwik, K. Berggold, H. Kierspel, O. Zabara, A. Freimuth, T. Lorenz, Phys. Rev. B 69 (2004) 094417.
[18] Y. Sun, X.J. Xu, Y.H. Zhang, Phys. Rev. B 62 (2000) 5289.
[19] K. Asai, O. Yokokura, N. Nishimori, H. Chou, J.M. Tranquada, G. Shirane, S. Higuchi, Y. Okajima, K. Kohn, Phys. Rev. B 50 (1994) 3025.
[20] M.A. Korotin, S.Yu. Ezhov, I.V. Solovyey, V.I. Anisimov, D.I. Khomskii, G.A. Sawatzky, Phys. Rev. B 54 (1996) 5309.
[21] S. Yamaguchi, Y. Okimoto, Y. Tokura, Phys. Rev. B 55 (1997) R8666.
[22] C. Zobel, M. Kriener, D. Bruns, J. Baier, M. Gruninger, T. Lorenz, P. Reutler, A. Revcolevschi, Phys. Rev. B 66 (2002) 020402(R).
[23] G. Maris, Y. Ren, V. Volotchaev, C. Zobel, T. Lorenz, T.T.M. Palstra, Phys. Rev. B 67 (2003) 224423.
[24] S.R. English, J. Wu, C. Leighton, Phys. Rev. B 65 (2002) 220407.
[25] J. Wu, C. Leighton, Phys. Rev. B 67 (2003) 174408.
[26] B. Roy, S. Das, J. Alloy Compd. 509 (2011) 5537.
[27] J.C. Debnath, R. Zeng, J.H. Kim, S.X. Dou, J. Magn. Magn. Mater. 323 (2011) 139.
[28] N. Dhahri, A. Dhahri, K. Cherif, J. Dhahri, H. Belmabrouk, E. Dhahri, J. Alloy Compd. 507 (2010) 405.
[29] H. Szymczak, R. Szymczak, M. Baran, J.F. Finowicki, J. Magn. Magn. Mater. 272–276 (2004) 1327.
[30] A.M. Aliev, A.G. Gamzatov, A.B. Batdalov, V.S. Kalitka, A.R. Kaul, J. Alloy Compd. 509 (2011) L1–L3.
[31] S.C. Ma, Q.Q. Cao, H.C. Xuan, C.L. Zhang, L.J. Shen, D.H. Wang, Y.W. Du, J. Alloy Compd. 509 (2011) 1111.
[32] L. Li, K. Nishimura, H. Igawa, D. Huo, J. Alloy Compd. 509 (2011) 4198.
[33] X.H. Liu, W. Liu, S. Guo, W.J. Gong, X.K. Lv, Z.D. Zhang, J. Alloy Compd. 507 (2010) 26.
[34] G.H. Meng, O. Tegus, W.G. Zheng, L. Song, J.H. Huang, J. Alloy Compd. 497 (2010) 14.
[35] M.C. Ma, D.H. Wang, C.L. Zhang, H.C. Xuan, S.D. Li, Z.G. Huang, Y.W. Du, J. Alloy Compd. 499 (2011) 7.
[36] J.J. Ipus, J.S. Blázquez, V. Franco, A. Conde, J. Alloy Compd. 496 (2010) 7.
[37] A.K. Kundu, P. Nordblad, C.N.R. Rao, Phys. Rev. B 72 (2005) 144423.
[38] N. Orlovskaya, D. Steinmetz, S. Yarmolenko, D. Pai, J. Sankar, J. Goodenough, Phys. Rev. B 72 (2005) 014122.
[39] M. An, S.K. Yuan, Y. Wu, Q.M. Zhang, X.G. Luo, X.H. Chen, Phys. Rev. B 76 (2007) 024305.
[40] A. Ishikawa, Phys. Rev. Lett. 93 (2004) 136401–136404.
[41] W.J. Luo, F.W. Wang, Appl. Phys. Lett. 90 (2007) 162515.
[42] J. Geshev, Appl. Phys. Lett. 93 (2008) 176101.
[43] J.Z. Sun, L. Krusin-Elbaum, A. Gupta, Gang Xiao, S.S.P. Parkin, Appl. Phys. Lett. 69 (1996) 1002.
[44] R. Caciuffo, D. Rinaldi, G. Barucca, J. Mira, J. Rivas, M.A. Senaris-Rodrigues, R.G. Radaelli, D. Floriani, J.B. Goodenough, Phys. Rev. B 59 (1999) 1068.